Self-Consistent Field and Motion of Electrons Which Have a Range in Canonical Angular Momentum in a Uniform Magnetic Field*

LEWI TONKS†
Lawrence Radiation Laboratory, University of California, Livermore, California
(Received November 2, 1959)

The self-consistent theory of relativistic electrons circulating in a uniform impressed magnetic field, the "Astron problem," has been generalized to the extent that a range of canonical angular momentum among monoenergetic electrons has been treated. For simplicity, the density distribution in phase space has been chosen to be uniform over a finite momentum range. Just as in the single-momentum case, field reversal is found, but new field and spatial density configurations appear. The uniform distribution is found to be consistent with isotropic regions of constant spatial density and constant magnetic field. The thickness of transition layer between vacuum and such a region conforms, within limits, to an empirical relation previously found. The limit to the number of electrons per unit axial length of layer still exists. The curves relating the ratio of internal to external field to the layer strength still show multiple values of both ratio and strength in certain ranges. Trajectories have been calculated and plotted for several cases.

I. INTRODUCTION

THE first step toward the solution of the theoretical problem posed by the layer of relativistic electrons which are expected to generate the magnetic field reversal required for the Astron has been taken in a previous report, hereafter to be designated by I.[1] The next logical step was to broaden the problem to include a range in an electron parameter and, in view of the method of attack, the parameter chosen was the canonical angular momentum. An important purpose served by this step has been to relate the assumed distribution-in-momentum to distribution in space, energy, direction of motion, etc. The need lies, to quote I, in the fact that "the essential difficulty (in the theoretical approach) is the setting up of the distribution function to correspond to a physical situation."

II. MATHEMATICAL FORMULATION

The motion of the electrons was, as in I, considered to be confined to the r, θ plane but to lie in a relativistic range. Purely for convenience their charge was taken to be positive. The distribution function for the density in constant-of-the-motion space was taken, quite generally, to be (with its attendant space element)

$$f_c(p,p_\theta)dpdp_\theta, \tag{1}$$

where p is the linear momentum and p_θ is the canonical angular momentum (CAM). This function, whose integral over p and p_θ is the number of electrons per axial cm, had to be related to the function which was useful in the self-consistency analysis. The latter was the density distribution in coordinate-momentum space expressed in terms of the constants of the motion. These were p, p_θ and, say, two position coordinates α_1 and α_2 at time zero. The number of electrons in an element of this phase space could therefore be represented as

$$f_1(p,p_\theta,\alpha_1,\alpha_2)drdp_rd\theta dp_\theta, \tag{2}$$

where p_r is the radial component of momentum.

Before establishing the relationship between f_c and f_1 two simplifying changes of notation were made. First, the magnetic part of CAM was expressed as an angular momentum:

$$p_B(r)\equiv(e/c)rA_\theta(r), \tag{3}$$

so that

$$p_\theta=pr\sin\phi+(e/c)rA(r)=pr\sin\phi+p_B(r), \tag{4}$$

where ϕ is the obliquity of the trajectory to the radius vector, I, Fig. 1. Second, all momenta $p, \cdots$ were replaced by $P, \cdots$ by means of the substitution

$$(P, \cdots)\equiv(p, \cdots)/m_0c. \tag{5}$$

Thus we could start afresh with an

$$f_c(P,P_\theta)dPdP_\theta, \tag{6}$$

and an

$$f_1(P,P_\theta,\alpha_1,\alpha_2)drdP_rd\theta dP_\theta. \tag{7}$$

The formula for resultant (linear) momentum became

$$P^2=P_r^2+[P_\theta-P_B(r)]^2/r^2. \tag{8}$$

The electrons of expression (7) had to be summed over r and θ, but first, in order to relate f_1 to f_c, it was necessary to separate out a common differential element, $dPdP_\theta$, with expression (6). This was done by using Eq. (8):

$$dP_r=(\partial P_r/\partial P)dP=Pr[P^2r^2-(P_\theta-P_B)^2]^{-\frac{1}{2}}dP. \tag{9}$$

(The more general 4-component Jacobian reduces to this.)

The integration of expression (7) over r and θ in the magnetic field defined by $P_B(r)$ could then be carried

* Work was performed under auspices of the U. S. Atomic Energy Commission.
† Consultant to the University of California Radiation Laboratory, Livermore, California under contract with the Atomic Power Equipment Department, General Electric Company and Lewi Tonks.
[1] L. Tonks, Phys. Rev. 114, 637 (1959).

out with the result that

$$2\pi\left(\int_{\text{cycle}}\{1-[P_\theta-P_B(r)]^2/P^2r^2\}^{-\frac{1}{2}}dr\right)\times f_1(P,P_\theta,\alpha_1,\alpha_2)dPdP_\theta=f_c(P,P_\theta)dPdP_\theta. \quad (10)$$

It was immediately evident that f_1 did not depend on α_1 and α_2 so that these quantities could be dropped. The limits of the integral had to be such that the full range of P_r was covered. In terms of r this required a full cycle of its values in the trajectory, that is, a doubling of the integral between pericenter and apocenter. Henceforward this would be the integral which was to be understood—as a consequence 2π would be replaced by 4π.

Since the assumption was that the electrons were monoenergetic, neither f_c not f_1 contained P explicitly, and each could be considered to contain a $\delta(P-P_0)$ factor, where P_0 corresponds to the energy. Then integration over P could be carried out, and, without ambiguity, the integral of Eq. (10) could be written

$$4\pi\int(\{1-[P_\theta-P_B]^2/P_0^2r^2\}^{-\frac{1}{2}}dr)\times f_1(P_\theta)dP_\theta=f_c(P_\theta)dP_\theta. \quad (11)$$

The differential electric current was then expressed by combining the speed $cP(P^2+1)^{-\frac{1}{2}}$ and the obliquity of the trajectory, ϕ, (see I, Fig. 1) with the revised function $\delta(P-P_0)f_1(P_\theta)$:

$$dj=ecP(P^2+1)^{-\frac{1}{2}}\sin\phi\delta(P-P_0)\times f_1(P,P_\theta)drdP_rd\theta dP_\theta, \quad (12)$$

Also

$$\sin\phi=(P_\theta-P_B)/Pr. \quad (13)$$

Then by using Eq. (9) it was possible to integrate Eq. (12) over P to give

$$\frac{ecP_0[P_\theta-P_B(r)]f_1(P_\theta)drd\theta dP_\theta}{[P_0^2+1]^{\frac{1}{2}}\{1-[P_\theta-P_B(r)]^2/P_0^2r^2\}^{\frac{1}{2}}}. \quad (14)$$

The choices of density distribution, f_1, which allowed of a straightforward rather than an iterative solution for self-consistency were ones which permitted an immediate integration of expression (14) with respect to P_θ. The only choice was to make $f_1(P_\theta)$ a constant over a range of P_θ:

$$\begin{aligned} &f_1(P_\theta)=0 \quad \text{for} \quad P_\theta<P_a \quad \text{and} \quad P_\theta>P_b, \\ &f_1(P_\theta=\alpha \quad \text{for} \quad P_a<P_\theta<P_b. \end{aligned} \quad (15)$$

This was a frankly arbitrary choice. Any direct choice of an f_1 would have been equally arbitrary because the chosen function would not have arisen from a physical situation, except by the purest chance. The realistic approach would have had to begin with a calculation of f_c, as will be done when the E layer resulting from slowing-down electrons is calculated. The justification for the present procedure lay, first, in the relative ease with which it allowed some qualities of a field-reversing layer to be examined qualitatively and, second, in its being a stepping stone to the considerably more involved iterative procedure required to link f_c and f_1 to the physics situation.

Then the integral of expression (14) with respect to P_θ gave for the differential current of current density j:

$$jrdrd\theta=-\frac{2ecP_0^2\alpha}{(P_0^2+1)^{\frac{1}{2}}}\left\{\left[1-\left(\frac{P_b-P_B}{P_0r}\right)^2\right]^{\frac{1}{2}}-\left[1-\left(\frac{P_a-P_B}{P_0r}\right)^2\right]^{\frac{1}{2}}\right\}rdrd\theta, \quad (16)$$

where the factor 2 enters in essentially the same way as in Eq. (10).

It was then convenient to introduce the function $R_i(r)$, similar to the R of I, which was characteristic of trajectory i, for which $P_\theta=P_i$,

$$R_i(r)\equiv-\sin\phi_i(r)\equiv-[P_i-P_B(r)]/P_0r. \quad (17)$$

The negative sign was, as in I, appropriate to dealing with a positive electronic charge and picturing specific situations on this basis. Then

$$jrdrd\theta=-\frac{2ecP_0^2\alpha}{(P_0^2+1)^{\frac{1}{2}}}[(1-R_b^2)^{\frac{1}{2}}-(1-R_a^2)^{\frac{1}{2}}]rdrd\theta.$$

From Eqs. (3) and (5)

$$rA_\theta(r)=(m_0c^2/e)P_B(r)=(m_0c^2/e)(P_0rR_i+P_i),$$

and it appeared that

$$d(rA)/dr=(m_0c^2P_0/e)d(rR)/dr,$$

independent of trajectory, so that Maxwell's equation

$$\frac{d}{dr}\left(\frac{d[rA_\theta(r)]}{rdr}\right)=-4\pi j/c,$$

became

$$\frac{d}{dr}\left(\frac{d(rR_b)}{rdr}\right)=-\frac{8\pi e^2\alpha P_0}{m_0c^2(P_0^2+1)^{\frac{1}{2}}}\times[(1-R_b^2)^{\frac{1}{2}}-(1-R_a^2)^{\frac{1}{2}}], \quad (18)$$

with

$$R_a(r)=R_b(r)+(P_b-P_a)/P_0r. \quad (19)$$

A simplifying substitution was

$$t\equiv\left(\frac{8\pi e^2\alpha P_0}{m_0c^2(P_0^2+1)^{\frac{1}{2}}}\right)^{\frac{1}{2}}r=\left(\frac{8\pi r_e\alpha}{\gamma}\right)^{\frac{1}{2}}r=\frac{t_2}{r_2}r, \quad (20)$$

where r_e is the classical electron radius and γ is m/m_0 and the subscript 2 refers to values at the external

radius of the electron layer. Equation (18) then became

$$\frac{d}{dt}\left(\frac{d(tR_b)}{tdt}\right)=(1-R_b^2)^{\frac{1}{2}}-(1-R_a^2)^{\frac{1}{2}}, \qquad (21)$$

and this is the fundamental differential equation of the problem. Like the variable s in I, the t here was to be regarded as a mathematical parameter. As in I a dimensionless "magnetic field," h, was introduced:

$$th\equiv\frac{d(tR_b)}{dt}=\frac{dP_B(r)}{P_0dr}=\frac{e}{mvc}rB,$$

where v is the electron speed and m its relativistic mass.

Quite analogously to the single-type case, the quantity

$$G\equiv t_2h_2=r_2/a_2 \qquad (22)$$

was defined, a_2 being the radius of the electron gyration in the field B_2. The value of G together with a value for t_2 and the value -1 for R_b constitute the initial conditions for a solution.

Besides G another physics parameter is, as in I, the total number N of electrons per cm of axial length. This was found by integrating Eq. (11):

$$N=\int f_c(P_\theta)dP_\theta.$$

The integral of the left member of Eq. (11) with respect to P_θ could be performed over the range P_a to P_b so that

$$N=4\pi P_{0\alpha}\int r(\cos^{-1}R_b-\cos^{-1}R_a)dr, \qquad (23)$$

or

$$\nu\equiv(2r_e/\gamma)N=\int t(\cos^{-1}R_b-\cos^{-1}R_a)dt. \qquad (24)$$

The magnetic field is represented by

$$h\equiv\frac{d(tR)}{tdt}=\frac{(P_0^2+1)^{\frac{1}{2}}B}{P_0(8\pi\alpha m_0c^2)^{\frac{1}{2}}}=\frac{B}{(8\pi\alpha mv^2)^{\frac{1}{2}}}. \qquad (25)$$

The stated limits, P_a and P_b, in the integration of Eq. (11) to obtain Eq. (23), and in the integration of Eq. (14) to obtain Eq. (16) were imposed by the types of electrons in the system, but certain ranges of r are inaccessible to some of these types, and this circumstance is made evident by an imaginary value for the integrand. Thus, near enough to the outside of the electron layer there are no P_a electrons and the range of integration in the evaluation of f_1 there extends from P_b down to the value of P_θ for which the denominator vanishes. Further in, the upper limit, too, may be fixed by a zero of the denominator.

In general it was not difficult to determine that whenever $|R|>1$ then, in Eq. (21) $1-R^2$ was to be replaced by zero and in Eq. (24) $\cos^{-1}R$ was to be replaced by 0 if $R>1$ and by π if $R<-1$.

Both Eqs. (21) and (24) could be expressed in terms of momentum range by means of Eq. (19) rewritten as:

$$R_a=R_b+\Delta Q/t, \qquad (26)$$

with

$$\Delta Q\equiv[(P_b-P_a)/P_0](t_2/r_2). \qquad (27)$$

Furthermore it was convenient to characterize an orbit by Δq instead of P_θ where

$$\Delta q\equiv\Delta Q(P_b-P_\theta)/(P_b-P_a), \qquad (28)$$

so that Δq lies in the range 0 to ΔQ. If followed rather easily that the difference in obliquity of two trajectories at the same radius is just their $\Delta q/t$.

It was apparent that the two parameters, t_2 and G, had the same roles as s_2 and g_2 before, and, in addition, we had ΔQ which measures the momentum spread. This made the problem more complex.

Since p_θ differs from trajectory to trajectory, it was helpful to relate the change in p_θ to the change in trajectory in a general way. First, we focused on the radial position, r_A, of the apocenter. At this point $\sin\phi=-1$. From Eq. (4) we had

$$dp_\theta/dr_A=p_0[er_AB(r_A)/p_0c-1]=p_0(r_A/a_A-1),$$

where a_A is the radius of gyration at the apocenter. Necessarily at the apocenter

$$r_A>a_A,$$

so that for our basic conditions (positive particles in a positive field) where p_θ decreased the apocenter moved inward, as indicated by radial arrows at the apocenters in Fig. 1.

With regard to the pericenter four cases needed to be distinguished according to the local values of

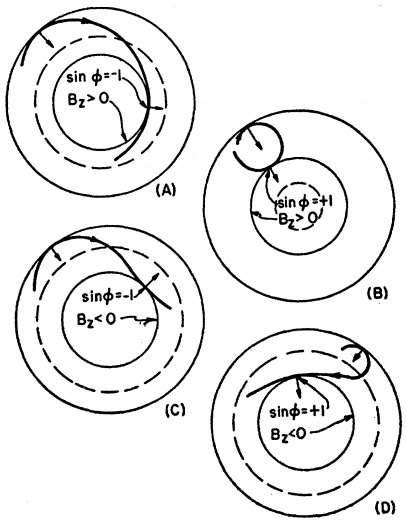

FIG. 1. Types of trajectories having maximum canonical angular momentum.

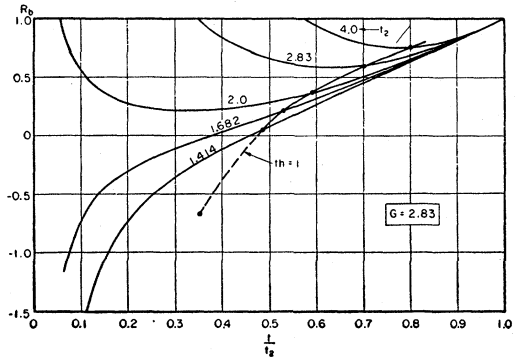

FIG. 2. Trajectory obliquity, R_b, as a function of relative radial distance for $G=2.83$ and various t_2; also position of equilibrium orbit.

$\sin\phi$, which can be either ∓ 1, and of B_z, which can be either positive or negative. The cases are distinguished by the shape of the trajectory of the p_b electrons which can be of any one of four corresponding types. They are shown in Fig. 1. Systematic substitution of the pertinent pericenter values of $\sin\phi$ and B_z in the derivative of Eq. (4), as was done for the apocenter, established the radial arrows at the pericenters, which show the shift in trajectory there for a decrease in p_θ.

A little consideration showed that in all cases the smallest value of p_θ attainable is that reached when $r/a=1$, which would always be in a region of positive field, and is shown qualitatively by the broken-circle trajectories. Quantitatively the radius, r_c, of this minimum-p_θ circular orbit is fixed by the equation

$$er_cB(r_c)=p_0c, \quad \text{or} \quad t_ch_c=1.$$

It is the "equilibrium" orbit of accelerator theory and that is what it will be called here.

To sum up in admittedly qualitative fashion, we see that in a magnetic field strong enough to establish a well-defined guiding center for the maximum-p_θ trajectory as in Case B of Fig. 1, a downward range of p_θ corresponds to a distribution of guiding centers extending inward toward the axis. In all other cases the downward range of p_θ corresponds to a decreasing amplitude of oscillation about the equilibrium orbit. In all cases the equilibrium orbit corresponds to the least possible p_θ. This description applies, of course, only to the special assumptions of the present analysis, particularly that $p=p_0$. At a later stage of the general inquiry we shall be interested in slowing down, and then a possible minimum value for p_θ might be that of a particle at rest where $B=0$.

Equation (21) was solved from the outer surface of the electron layer, just as for I, so that a choice of the two parameters t_2 and G had to be made. A decision regarding the momentum spread, characterized by ΔQ, was postponed by noting that a large ΔQ could, by keeping $R_a>1$ by virtue of Eq. (27), put off the point at which the second term of the right member became active. As the solution proceeded on this basis, fresh electrons were continually encountered and incorporated by the mathematics in accordance with Eq. (15), and at some point the exclusion of old electrons would begin. The limit to the assimilation part of this process was imposed by the value of p_θ corresponding to the equilibrium orbit, for this was the smallest value which could be present and hence the smallest value which could be attributed to p_a. As the solution proceeded to still smaller radii, electrons of ever-larger p_θ were excluded until either the axis was reached or the p_b electrons themselves were excluded, whichever occurred first. If it was the latter, only uniform vacuum field remained inside.

Figures 2 and 3 show the behavior of R_b and h/h_2 when Eq. (21) was solved omitting the R_a term. On each plot the curve marked "$th=1$" is the locus of equilibrium-orbit radii. The value of p_a which is consistent with these curves is that which would cause $R_b+\Delta Q/t$ in Eq. (26) just to reach unity, in which case the R_a term in Eq. (21) just misses entering the calculation. The crucial radius lies on the "$th=1$" curve. Thus, the curves of Figs. 2 and 3 apply to the physical situation where all momenta from the maximum p_b to the minimum possible are present, and all trajectories from that with maximum apocenter distance to the minimum-momentum "equilibrium" orbit are there.

With this physics interpretation at hand it was throught advisable to avoid the complication of a third parameter; and, except in two particular cases, to deal in the calculations only with a full range of momenta, that is, with $\Delta Q=\Delta Q_m$, its maximum possible value.

As we have noted, for the equilibrium orbit

$$1=t_ch_c=d(tR_b)/dt|_c=R(t_c)+t_cR_b'(t_c). \tag{29}$$

For ΔQ_m we also have

$$1=R_b(t_c)+\Delta Q_m/t_c,$$

whence

$$\Delta Q_m=t_c[1-R_b(t_c)]=t_c^2R_b'(t_c). \tag{30}$$

In calculating and tabulating ΔQ_m it has not been necessary to distinguish between cases A, B, C, and D of Fig. 1, but for other reasons it is necessary to dif-

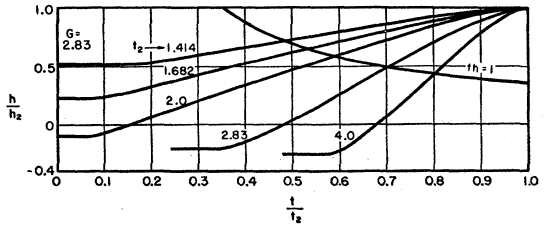

FIG. 3. Relative field strength as a function of relative radial distance for $G=2.83$ and various t_2 with full range of momentum; also position of equilibrium orbit.

ferentiate between the resulting configurations. In B the whole space within the outermost locus of apocenters is populated by electrons, and any restriction of ΔQ to a value less than ΔQ_m will first depopulate the annular neighborhood of the equilibrium orbit and this attenuation will spread inward and outward with decreasing ΔQ. A possible later stage is one in which vacuum at the axis progresses outward but never reaches beyond the pericenters of the p_b electrons. Then only p_b electrons would be present, as in I. In A and C only the space between the loci of apocenters and pericenters of the p_b electrons, as indicated, are populated, and the maximum density lies close to the equilibrium orbit. Any decrease in ΔQ below ΔQ_m in these cases will again depopulate the annular neighborhood of the equilibrium orbit, at the same time causing the magnetic field to the interior of the depopulated region to increase positively. In D, as in B, the whole region inside the p_b apocenters is populated, and here also the diminishing of ΔQ depopulates the annular neighborhood of the equilibrium orbit initially.

In the first three cases, A, B, and C, the decrease of ΔQ is seen to cause the configurations to approach types already found in I for single-type electrons, just as would be expected. It is, of course, the p_b trajectory which shows the similarity. D, however, is essentially new. Its p_b trajectory is, as a whole, paramagnetic so that to reverse the field, as occurs here, the trajectories of lower p_θ, many of which do not reverse their direction of circulation about the axis, must outweigh the near-p_b trajectories. In A and C, as low-p_θ trajectories are eliminated, one can think of compensating by increasing the total layer strength, but in D this is not possible because of the paramagnetism of the near p_b electrons. Therefore, the removal of the low p_θ electrons must lead to a positive increment to the interior field and the evolution will be toward B. This is illustrated in Fig. 6.

Because of this new configuration it was thought to be worth-while to calculate a few trajectories. From

$$r\dot{\theta}=v\sin\phi, \quad \dot{r}^2+(r\dot{\theta})^2=v^2,$$

it followed directly that

$$\frac{d\theta}{dr}=\frac{-R}{r(1-R^2)^{\frac{1}{2}}}, \qquad \frac{d\theta}{d(t/t_2)}=\frac{-R}{(t/t_2)(1-R^2)^{\frac{1}{2}}}, \tag{31}$$

Having calculated and tabulated R_b, any other trajectory followed easily by using the appropriate Δq and setting

$$R=R_b+\Delta q/t.$$

A quadrature by machine gave t/t_2 as a function of θ.

In I the intersection of the axis by a trajectory was a very special case. Here, because of the spread in p_θ that always happens for configurations of types B and D of Fig. 1. The special cases are those in which it is the p_b trajectory which reaches to the center so that $R_b(0)=0$. Attention was confined to the case where the full range of p_θ was present so that the differential equation is, as before, Eq. (21) without the R_a term, and the series solution near $t=0$ is

$$R_b=(h_0/2)t+(1/3)t^2-(h_0^2/120)t^4-(h_0/144)t^5 -(1/70)(1/9+h_0^4/64)t^6+0(t^7).$$

Here h_0 is the value of h at $t=0$.

As in I, solutions of the singular case served to pinpoint ill behavior, as will appear. The pertinent range of h_0 is that within which R_b passes through $+1$ (rather than -1) at some value of t which is thus identified as t_2. It comprises values greater than approximately -2. The values of h_2, t_2, and ν corresponding to the G's of the regular solutions were found by interpolation.

To determine analytically how the solutions behave for large t_2 was less simple than in the earlier case, but the answer is the same for field ratio and layer strength, namely

$$h_1/h_2\to 2/G-1, \quad \nu\to 2(G-1).$$

This accords with the expectation that as the trajectories are forced to conform more and more closely to the injection circle of radius r_2 the effect on ν and h_1/h_2 of angular momentum distribution should be less and less. There should, however, be an effect on layer thickness. Let t_1 be the value of t at the pericenter of a p_b electron. The asumptotic relation for the layer thickness is then

$$\frac{t_2-t_1}{t_2}\simeq\frac{2}{t_2}\left(\frac{g_2-1}{t_2}\right)^{\frac{1}{2}},$$

which differs from I, and is approached more slowly.

III. GENERAL TABULATION OF RESULTS

A general complication of the results of calculating the spatial extent, the magnetic field ratio, "equilibrium" orbit and the layer strength, as well as identification of the configuration according to the classification of Fig. 1 is given in Table I. The arrangement is primarily according to increasing G, secondarily according to increasing t_2, and thirdly, when ΔQ is less than the maximum, according to decreasing ΔQ. The last-mentioned cases are designated by the letter u.

The numerical values used for G and t_2 were chosen to be commensurably spaced on a scale of $\log_2$ with the rough idea that linear interpolation on such a scale might be more accurate. Thus, the successive values of $\log_2 G$ are 1, 1.5, 1.75, 2, 3. Of course the singular solutions, Case S, do not fit this scheme.

The quantities tabulated and their sources are as follows: G, ratio of apocentral radius of p_b electrons to gyration radius in impressed vacuum field; t_2, math-

TABLE I. Results.

G	t_2	ΔQ_m and ΔQ	h_2	Case[a]	$R_b(t_1)$	t_{1a}/t_2	t_1/t_2	h_1/h_2	t_c/t_2	ν	U
2	1.000	0.2152	2.000	A	1		0.1016	0.6948	0.5690	0.3450	
	1.414	0.2683	1.414	A	1		0.1980	0.5151	0.6228	0.6028	
	2.000	0.3109	1.000	A	1		0.3500	0.3331	0.6966	0.9359	
	4.000	0.3353	0.500	A	1		0.6765	0.1178	0.8449	1.5126	
	8.000	0.3019	0.250	A	1		0.8632	0.0430	0.9329	1.8002	
	∞		0	S	0		0	0	1.0000	2.0000	
2.830	1.414	0.6461	2.001	B	−1		0.1581	0.5165	0.4894	1.1544	0.902
	1.682	0.7010	1.683	B	−1		0.0746	0.2248	0.5373	1.5147	0.802
	1.863		1.519	S	0		0	−0.0731		1.737	
	2.000	0.7435	1.415	C	1		0.0562	−0.1082	0.5922	1.8920	0.666
	2.830	0.7855	1.000	C	1		0.3478	−0.2081	0.7058	2.5312	
	4.000	0.7786	0.708	C	1		0.5756	−0.2490	0.8010	2.9549	
	∞		0				1.0000	−0.2933	1.0000	3.6600	
3.364	1.000	0.7386	3.364	B	−1		0.3691	0.8515	0.3491	0.7503	
	2.000	1.0720	1.682	B	−1		0.1680	0.1822	0.5342	2.5213	
	2.310		1.456	S			0	−0.432		2.984	
	2.378	1.1106	1.415	C	1		0.0371	−0.4283	0.6021	3.0620	
	2.432	1.1142	1.383	C	1		0.0652	−0.4255	0.6098	3.1172	
	2.830	1.1277	1.189	C	1		0.2360	−0.4154	0.6681	3.4417	
	4.000	1.1105	0.841	C	1		0.5203	−0.4090	0.7782	3.9454	
	∞		0				1.0000	−0.4055	1.0000	4.7280	
4.000	1.000	1.0264	4.000	B	−1		0.4777	0.8971	0.2787	0.8655	0.990
		u0.8656	4.000		−1	0.038	0.480	1.0024	0.2634	0.7362	
		u0.6733	4.000		−1	0.190	0.480	1.0011	0.2524	0.5685	
		u0.4107	4.000		−1	0.330	0.487	1.0004	0.2499	0.3417	
	2.000	1.5147	2.000	B	−1		0.3728	0.4981	0.4588	3.1793	0.938
	2.378	1.5653	1.682	B	−1		0.2528	0.1405	0.5422	4.1356	0.852
	2.594	1.5781	1.542	D	−1		0.1104	−0.2683	0.5851	4.5086	
		u1.3880	1.542		−1	0.251	0.275	0.3891	0.5220		
		u0.8850	1.542		−1	0.241	0.399	1.0212	0.2451		
	2.727		1.467	S	0		0	−0.7076		4.64	
	2.830	1.5834	1.413	C	1		0.0692	−0.6696	0.6242	4.7125	
	3.084	1.5823	1.297	C	1		0.1964	−0.6208	0.6604	4.8664	
	3.362	1.5756	1.190	C	1		0.2980	−0.5927	0.6940	4.9997	
	4.000	1.5484	1.000	C	1		0.4570	−0.5602	0.7533	5.2194	
	8.000	1.3428	0.500	C	1		0.7926	−0.5172	0.8994	5.7011	0.865
	16.000	1.1017	0.250	C	1		0.9186	−0.5061	0.9597	5.8835	0.948
	∞		0				1.0000	−0.5000	1.0000	6.0000	
8.000	2.000	5.5154	4.000	B	−1		0.7374	0.8967	0.1394	4.7663	0.995
	2.830	6.8656	2.826	B	−1		0.7214	0.7804	0.1602	9.4211	0.992
	4.000	6.6224	2.000	B	−1		0.6683	0.4795	0.2607	18.144	0.982
	4.757	5.2203	1.682	D	−1		0.4456	−0.1173	0.6655	23.370	0.980
	4.82		1.66	S	0		0	−1.175		21.7	
	4.862	5.1646	1.645	C	1		0.1311	−1.0998	0.6816	20.395	
	4.967	5.1150	1.611	C	1		0.2279	−1.0519	0.6954	19.114	
	5.187	5.0235	1.542	C	1		0.3326	−0.9997	0.7196	17.806	
	5.656	4.8606	1.414	C	1		0.4555	−0.9408	0.7597	16.553	0.17
	16.000	3.4582	0.500	C	1		0.8890	−0.7797	0.9454	14.260	0.832
	64.000	2.1897	0.125	C	1		0.9830	−0.7543	0.9915	14.031	0.992
	∞		0				1.0000	−0.7500	1.0000	14.000	

[a] See Fig. 1 for Cases A, B, C, and D. The letter S denotes the singular case.

ematical parameter, designating radius of apocenters of p_b electrons, Eq. (20); h_2, parameter designating impressed magnetic field, Eq. (25); ΔQ_m (and ΔQ), measure of spread of angular momentum, Eq. (30); $R_b(t_1)$, $+1$ when p_b electron is moving clockwise at pericenter, -1 when counter-clockwise, integration of Eq. (21); t_1, in t_1/t_2, parameter designating pericentral radius of p_b electron, integration of Eq. (21); t_{1a}, in t_{1a}/t_2, parameter designating pericentral radius of p_a electrons; h_1, in h_1/h_2, parameter designating magnetic field at $t \leqq t_1$, Eq. (25); t_c, in t_c/t_2, parameter designating radius of "equilibrium" orbit and the value of t_{1a} when p_a has minimum possible value, Eq. (29); the case is determined from the signs of $R_b(t_1)$ and h_1 according to Fig. 1; ν, the strength of the electron layer, Eq. (24); and U, parameter relating to depth of transition layer, Eq. (32).

In those cases where $\Delta Q < \Delta Q_m$ values were chosen for ΔQ to obtain a representative sampling. In the $4/1/\Delta Q_m$ case (designating $G=4$, $t_2=1$, $\Delta Q=\Delta Q_m$) the electron layer is isotropic and uniformly dense inside t_1. A slight reduction in ΔQ reduces the population in an annulus including t_c; but the largest ΔQ chosen, i.e., 0.8656, is so great a reduction from ΔQ_m that no electrons lie within $t_{1a}=0.038\ t_2$ of the axis. The spreading of the internal vacuum with the decrease in momentum spread is apparent. Also, reminiscent of I is the enhancement of the internal vacuum field, shown by

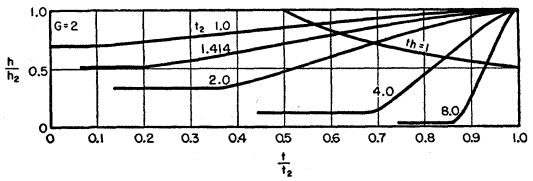

FIG. 4. Relative field strength as a function of relative radial distance for $G=2.0$ and various t_2 with full range of momentum; also position of equilibrium orbit.

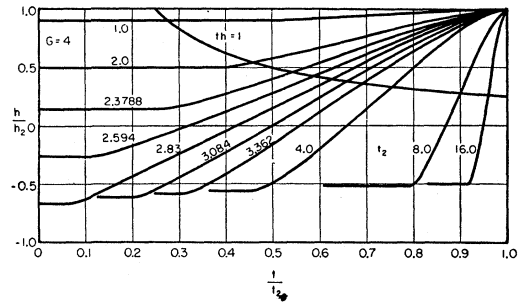

FIG. 5. Relative field strength as a function of relative radial distance for $G=4.0$ and various t_2 with full range of momentum; also position of equilibrium orbit.

$h_1/h_2>1$. It was of particular interest to explore an instance of Case D. This was done in the 4/2.594/1.5781 case. The shrinkage of ΔQ causes the uniform reversed field inside t_1 to be rectified, as was foreseen above, and a vacuum has developed inside t_{1a} when ΔQ has gotten down to 0.8850.

IV. FIELD DISTRIBUTION

Figures 3, 4, and 5 show the spatial magnetic field distribution in an interesting range of t_2 and G. No calculations were made for G less than 2, where field reversal is not possible. The calculations for $G=8$ showed nothing distinctive in this regard. It is immediately apparent that the distribution in p_θ has eliminated the cusp from the field curves. The singularities at beginning and end of the field transition region have receded from being infinite first derivatives to being infinite second derivatives, thus preserving the definiteness of this region while giving it a more physically plausible configuration.

There is a marked similarity between the present field distributions and those formed earlier[2] for a plane plasma (using a cruder method of analysis) where the two might be expected to be comparable. This is for Case B of Fig. 1, where, with the full range of p_θ present, there is an interior region of uniform unreversed field surrounded by a transition layer. This occurs when G is greater than 2 and t_2 is not too large.

One common feature is the existence of the region of homogeneous plasma and uniform field. Thus, the two assumptions, constancy of $\sigma(p)$ or $S(H)$ in reference 2 and constancy of α here, the one being tantamount to assuming uniform spatial density, the other uniform density in angular-momentum phase space, are both consistent with homogeneous plasma. This is, of course, because in each case, the vector potential is a linear function of the appropriate coordinate in a uniform-field region. In the transition region the two assumptions are not equivalent, so even apart from the difference between Cartesian and cylindrical geometry, the similarities can only be qualitative.

It did seem worth-while to test the empirical relation expressed by Eq. (38) of reference 2 in the present context, namely, that the transition layer thickness is twice the gyration radius of a particle moving in a uniform magnetic field which is equal to the arithmetic mean between the vacuum and the uniform-plasma fields. If this relation is rigorous, then

$$U\equiv(G/4)(1+h_1/h_2)[1+R_b(t_1)t_1/t_2]=1, \quad (32)$$

an equation which is rather easily derived. The second factor introduces the average field and the third factor the transition-layer thickness for Case B.

The approach to conformity with Eq. (32) should be best when G is large, when the transition layer pertains to Class B and when it is less than half r_2 in thickness. Table I, in its last column, sets forth some of the results bearing on the above observations. It is interestint to note that thin layers pertaining to Case C conform also.

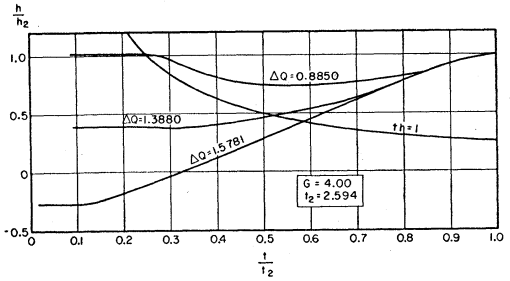

FIG. 6. Relative field strength as a function of relative radial distance for $G=4.0$, $t_2=2.594$ with partial ranges of momentum; also position of equilibrium orbit.

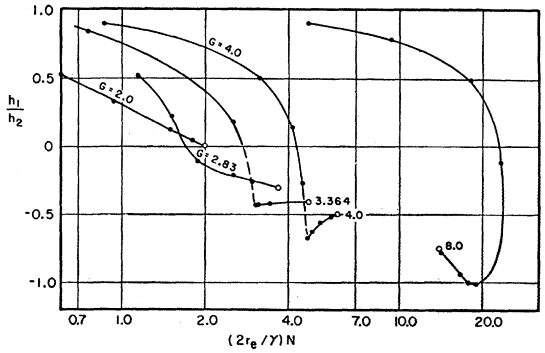

FIG. 7. The ratio of internal to external field as a function of layer strength with G as parameter.

[2] L. Tonks, Phys. Rev. 113, 400 (1959).

Figure 6 is the field distribution in the 4/2.594 cases where the momentum spread was varied. This shows the transition from field reversal to field enhancement for a Case D situation.

V. EFFECT OF LAYER STRENGTH; TRAJECTORIES

As was discussed in I, it is the layer strength $\nu - 2r_e N/\gamma$ there—which is to be regarded as the independent physics variable whereas t_2 serves as a mathematical parameter. Accordingly, in Fig. 7 the ratio of internal to vacuum field has been plotted against layer strength ν, and in Fig. 8 the same has been done with the ratio of pericentral to apocentral distances. For comparison Figs. 9 and 10 exhibit the same quantities in the same way for this case of single-type electrons, a portrayal unfortunately omitted from I.

In Fig. 7 the decrease of magnetic field is precipitous in a narrow range of ν although it is not discontinuous as it is in Fig. 9. There the discontinuity coincides with $s_1=0$; in Fig. 7 the cusp at the foot of the descent coincides with $t_1=0$. With increasing ν, it is just before the p_b trajectory reaches in to the axis that the field can reverse and the type D configuration is achieved.

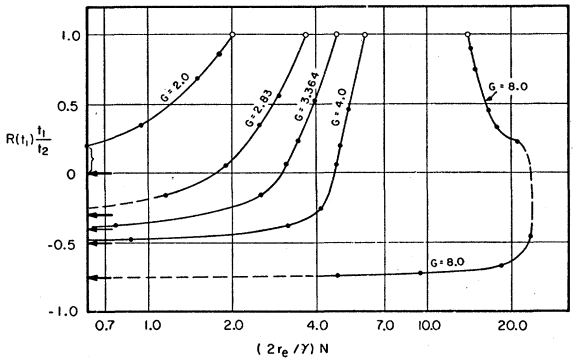

FIG. 8. The ratio of pericentral to apocentral distances, $R_b(t_1)t_1/t_2$, of maximum-p electrons as a function of layer strength with G as parameter.

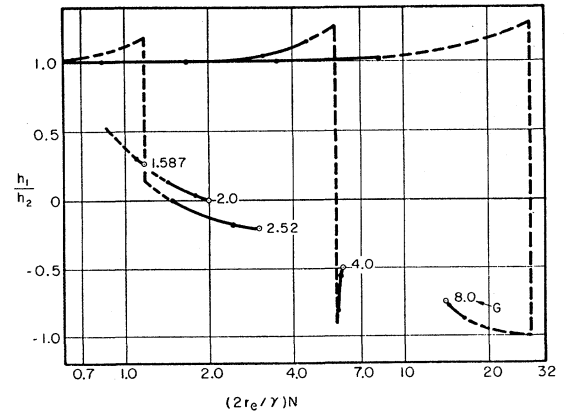

FIG. 9. For single-type electrons as in I, the ratio of internal to external field as a function of layer strength.

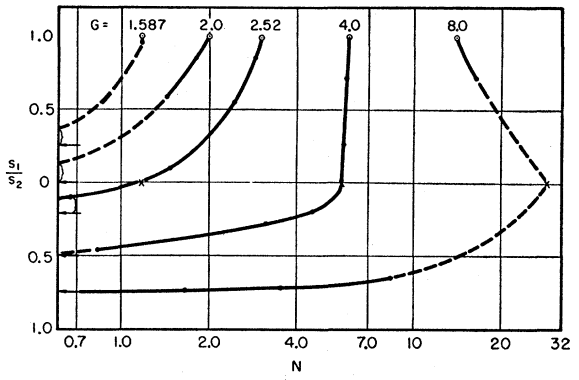

FIG. 10. For single-type electrons as in I, the ratio of pericentral to apocentral distances, $R(s_1)s_1/s_2$, as a function of layer strength.

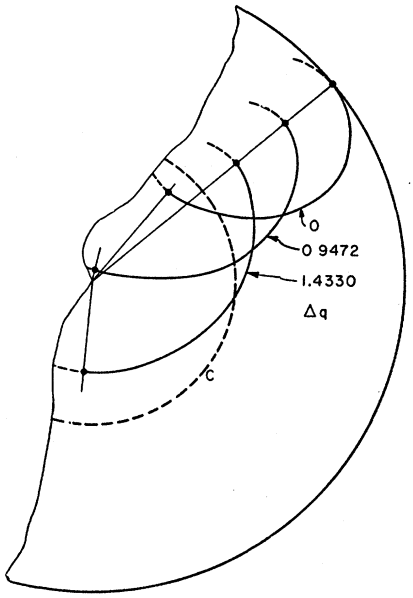

FIG. 11. Self-consistent trajectories for $G=4.0$, $\nu=3.180$. Case B of Fig. 1.

Beyond this although it seems reasonable that increasing the layer strength should enhance the reversed field ($G=2.83$), it is not clear why this should weaken it ($G=3.364$ and 4.0), or even be impossible ($G=8.0$) since ν already exceeds its asymptotic value. It is conceivable that all configurations up through $G=4$ would be stable, for there is only one configuration for each combination of G and ν, but it is inconceivable that all parts of the $G=8$ curves are stable and it is almost certain that it is the negative-field portion which is unstable.

Christofilos has pointed out[3] the importance of ν and has, on the basis of a simple thin-sheet picture of the E-layer, concluded that ν equals 2 for exact cancella-

[3] N. Christofilos, *Proceedings of the Second United Nations International Conference on the Peaceful Uses of Atomic Energy, Geneva, 1958* (United Nations, Geneva, 1958), Vol. 32, p. 280.

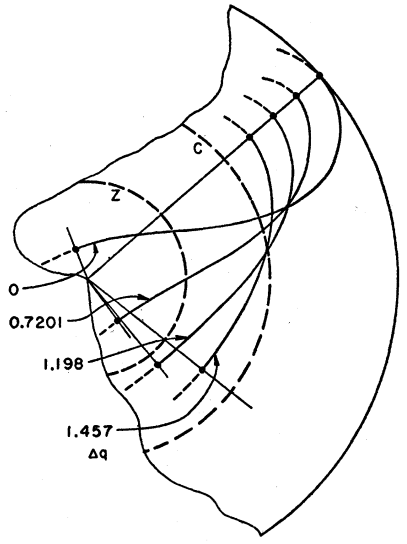

FIG. 12. Self-consistent trajectories for $G=4.0$, $\nu=4.510$. Case D of Fig. 1.

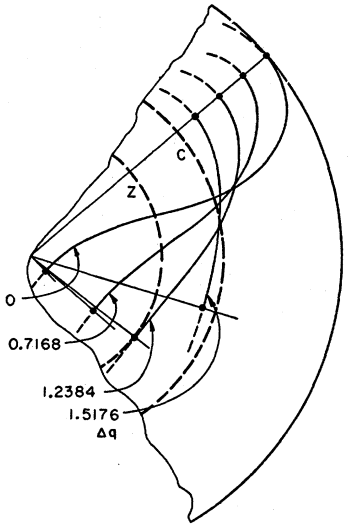

FIG. 13. Self-consistent trajectories for $G=4.0$, $\nu=4.712$. Case C of Fig. 1.

tion of the external vacuum field. Figures 7 and 9 show that the self-consistent E-layer does not conform to this simple relation.

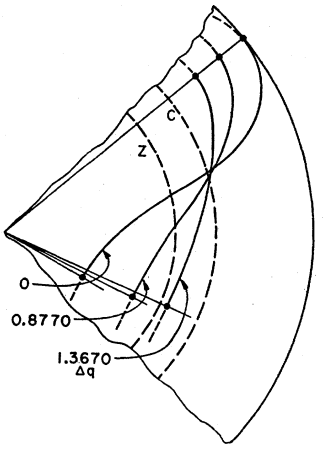

FIG. 14. Self-consistent trajectories for $G=4.0$, $\nu=5.000$. Case C of Fig. 1.

Figures 11 through 14 are families of trajectories illustrating Cases B, D, and C. Each trajectory is carried from apocenter to pericenter. The circle C, present in all cases, is the equilibrium orbit and the circle Z, present in Cases D and C, marks the zero-field position.

VI. CONCLUSION

The extension of the analytical method used in I to cover a range of angular momentum among monoenergetic electrons reveals some modification in form and characteristic of the self-consistent configurations. Field reversal still occurs even with the maximum range in momentum which is possible. Two configurations for a given layer strength, one with unreversed and one with reversed field are still present. In addition, the same h_1/h_2, reversed or unreversed, can be consistent with two different layer strengths. Undoubtedly stability considerations enter strongly.

The next step in the development of this area of consistent-field theory will be to allow initially monoenergetic electrons of identical angular momentum to slow down viscously in an ionized plasma, still neglecting scattering and the diamagnetism of the plasma.

It is a pleasure to acknowledge the contribution of Roy Clay of this Laboratory in carrying through from the mathematical equations to the numerical results on the IBM 650.